AIAA-2026-2684

Evolution of Wall-Bound Streamwise Vortices formed by a Spanwise Array of Surface Jets in a Turbulent Boundary Layer

Barnabas Toth[1], Bojan Vukasinovic[2] and Ari Glezer[3]
Georgia Institute of Technology, Atlanta, GA 30332-0405

Matthew C. DeFore[4] and Chris Harris[5]
Northrop Grumman Aeronautics Systems

The interactions of spanwise arrays of 3-D surface wall jets with the inner layer of a flat plate turbulent boundary layer are investigated in wind tunnel experiments. Each wall jets issues out of spanwise-rectangular embedded orifice that can be yawed relative to the free stream and the jet adheres to the surface by a Coanda-like effect along the downstream edge of the orifice and remains within the wall layer over 100 equivalent orifice diameters. While the evolution of a single jet varies significantly with its yaw angle (β = 0 and 60° are compared) spanwise arrays of adjacent straight and yawed jets can effect reasonably uniform distributions of near-wall gain in streamwise momentum albeit by different mechanisms and at different downstream distances from the jet orifices. While the momentum gain by each straight rectangular jet remains very close to the surface, the gain effected by the yawed jets spreads more in the cross-stream direction, reaching an asymptotic level of about 50% of the momentum deficit of the base boundary layer flow. Another characteristic element of the yawed jet array is that its evolution can be tailored by the interactions of the jets within the array with the leading and trailing jets (relative to the free stream direction) at the array's spanwise edges.

Nomenclature

C_q	=	mass flow rate coefficient
U_0	=	freestream velocity
d_e, d	=	(equivalent) jet diameter
Q	=	axial volumetric flowrate
TKE	=	turbulent kinetic energy
U	=	mean streamwise velocity
$\overline{u_i u_i}$	=	turbulent normal stress
$\overline{u_i u_j}$	=	turbulent shear stress
x	=	direction along the surface
y	=	direction normal to the surface
z	=	direction across the surface span
β	=	jet yaw orientation
Γ	=	circulation
Δ	=	jet spacing
$\Delta\varphi$	=	net change in momentum flux
δ	=	boundary layer thickness
δ^*	=	BL displacement thickness
θ	=	BL momentum thickness
ρ_0	=	free stream density
ϕ	=	through-plane momentum flux
ϕ_θ	=	BL through-plane momentum flux deficit
ω_x	=	streamwise vorticity component

1 Graduate Research Assistant, AIAA Member.
2 Research Engineer, AIAA Member.
3 Professor, AIAA Fellow.
4 Sr. Engineer, AIAA & INPSI Member.
5 Technology Development.

I. Introduction

Jets in cross flow are ubiquitous in a broad range of applications and have been studied extensively in numerous configurations over the years (e.g., Margason, 1993). The classical and most thoroughly studied example of jets in crossflow is the transverse jet, issuing normal and aligned in the direction of the cross flow where the boundary layer interaction with the jet results in the formation of a pair of counter-rotating vortices along the spanwise edges of the jet. Early investigations of the flow were motivated by atmospheric mixing, but they have rapidly evolved to include flows related to species mixing, cooling, aerodynamic maneuvering, etc., as outlined in detailed review articles by Mahesh (2013), Karagozian (2014), and Sharmishtha and Utpal (2017).

The use of circular surface jets for boundary layer control has been of specific interest in various aerospace applications and has been explored in several configurations over the last decades. Motivated by interest to utilize jets in cross flows as 'active' vortex generators in boundary layers over solid surfaces, Johnston and Nishi (1990) used surface-inclined jets for the deliberate formation of streamwise vortices of prescribed sense. They produced configurations of co- and counter-rotating vortices by inclined surface actuation jets that were yawed relative to the direction of the cross flow and noted the effect of jet yaw on delaying separation. In a follow-up investigation, Compton and Johnson (1992) reported that, while keeping the pitch angle $\alpha = 45°$, strongest vortices were generated at yaw orientations $45° < \beta < 90°$, and Johnston (1999) noted that at pitch angles below 45° strong, single-sense vortices are also formed at yaw within $60° < \beta < 90°$. In a later study, Milanovic and Zaman (2004) measured the flow downstream of highly inclined jets in a flat plate boundary layer over a range of yaw and pitch angles, jet momentum ratio and boundary layer thickness and characterized the peak streamwise vorticity, noting that highly yawed jets remain closer to the surface, enhance the turbulence intensity within the boundary layer, and reach their peak vorticity farther downstream. More recently, round vortex-generating jets have also been utilized in shock-wave boundary layer interactions that result in flow separation (e.g., Verma and Manisankar, 2019, Ramaswamy and Schreyer, 2021).

In contrast to the circular jets, there have been fewer investigations of vortices formed by jet with rectangular orifices. The review by Gutmark and Grinstein (1999) showed that most of the early works were motivated by mixing enhancement and the dynamics of the rectangular jets in the vicinity of the orifice. Motivated specifically by boundary layer flow applications and streamwise vortex generation, Zhang (2000) showed that rectangular jet at $\alpha = 30°$ and $0° < \beta < 135°$ yielded vortices exceeding the boundary layer height while the cores remained within the boundary layer and that at $\beta = 90°$ these jets produced stronger vortices than corresponding circular jets (the highest circulation was attained $\beta \approx 75°$ although it depended the streamwise position).

Initial jet-array studies also started with considerations of transverse jets. Sterland and Hollingsworth (1975) observed the effect of circular jet spacing in cross flow for transverse jets, and noted that penetration into the crossflow increased with decreasing jet spacing. In connection with the evolution of arrays of streamwise vortices, Pauley and Eaton (1988) showed that arrays of passively induced co-rotating vortices collectively deflect sideways within the boundary layer compared to a single vortex, arguably due to the combined effect of all their image vortices. Several investigations that focused on arrays of jets were motivated by film cooling applications. Berger and Liburdy (1998) considered compound jet orifices having either pitched or yawed exits and demonstrated that increased yaw resulted in well-defined flow structures that remained close to the surface. Findlay et al. (1999) examined the flow in the wake rectangular jets at $\alpha = 30°$ and

$\beta = 0°$ and 90° and reported that spanwise injection generated greater flow blockage and that if the jet spacing was small, such as 3 times the jet orifice width, it could prevent the formation of vortices at high blowing ratio. An array of inclined and swept jets also generates co-rotating vortices, whose merging behavior was characterized by the ratio of their core size and center to center distance a/b. With some variation, multiple studies indicated that the critical merging ratio was about $a/b = 0.3$, above which the vortex pairs became unstable and rapidly combined into a single vortex. Cerretelli and Williamson (2003) have shown that, in vortex merging away from a surface. the structure following merging was elliptical.

While the evolution of inclined, yawed jets in cross flow has been investigated extensively, few prior investigations considered the flow of such jets within a turbulent boundary layer (TBL) having a characteristic scale that is significantly larger than the scale of the jet. The present investigations build on earlier studies of yawed single and pairs of wall jets within a nominally 2-D TBL, and the formation and evolution of jet-induced vortices that remain bounded within the inner wall layer (Toth et al., 2025a, 2025b) with emphasis on the gain in distributions of spanwise momentum. The present work extends these studies by considering interactions of arrays of rectangular wall jets with the turbulent boundary layer and their disparate flow topologies at zero and nonzero yaw orientations.

II. Experimental Setup and Flow Diagnostics

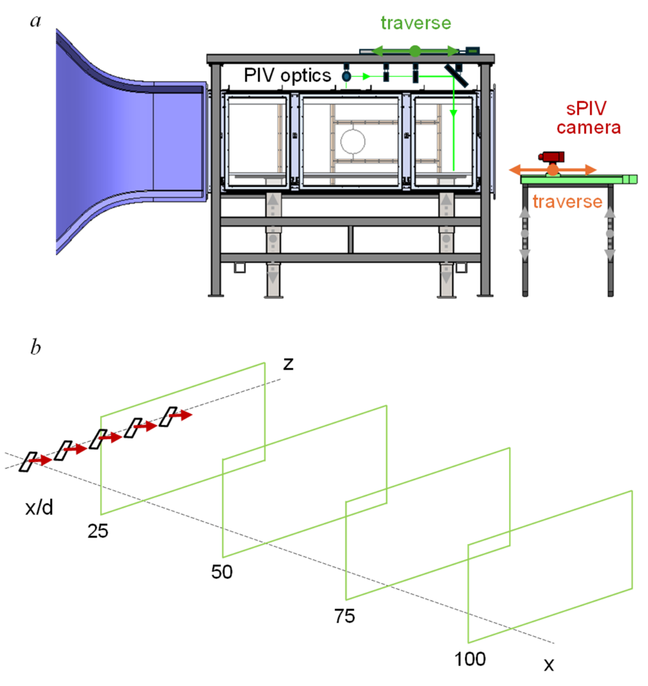

Figure 1. *Schematics of the experimental setup (a), and the stereo PIV measurement planes (b).*

The present investigations are conducted in an open-return, low-speed wind tunnel (Figure 1a) driven by a 150 HP blower (up to 95,000 CFM) with a 10:1 contraction downstream of a turbulence management section, having a square test section measuring 106 cm on the side and 304 cm in length that is optically transparent from three sides to enable optical measurements using PIV and flow visualization. The bottom wall of the test section was replaced with a horizontal flat plate model fabricated from a monolithic composite having a honeycomb core, sandwiched between two aluminum plates with bullnose half cylinder leading edge. The plate spans the full width of the tunnel's test section and is designed to be mounted so that it splits the airflow downstream of the contraction (Figure 1a) to form a spanwise-uniform boundary layer over its upper surface. The plate is attached on its lower surface to a light aluminum frame connected to four electric risers to enable adjustment of its elevation and streamwise inclination within the test section. Although in the present experiments the plate orientation is horizontal (zero pressure gradient), it can accommodate favorable and adverse streamwise pressure gradients. Stereo PIV measurements are acquired at the four streamwise-normal y-z planes $x/d_e = 25$, 50, 75 and 100 (relative to the center of the jet orifice), and the nominal PIV optical setup and the measurement planes are shown schematically in Figure 1. The jet orifice center ($x_0 = 0$), is set approximately 1,400d_e away from the leading edge of the plate.

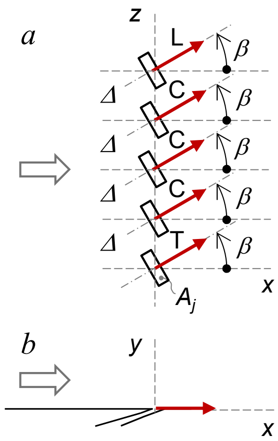

Figure 2. *a) Top viewof the leading and trailing rectangular wall jets with the yaw directions marked, and b) Cross-section of the wall jet orifice.*

The plate incorporates an opening with an interchangeable module that houses a spanwise array of five flush mounted rotatable cylindrical jet inserts so that their yaw relative to the free stream β can be independently varied, as illustrated in the top view Figure 2a (the pitch angle α is nearly zero by design, Figure 2b). Based on the evolution of a single jet, the jets' spacing is fixed at about $\Delta = 20d_e$ to allow adjacent jet interactions within $x/d_e = 100$. As illustrated in Figure 2a, the edge jets in the arrays are marked L (Leading), when the end jet issues towards the oncoming boundary layer flow and T (Trailing) when the end jet issues towards the neighboring jet. The jets within the array that are bound by the neighboring jets are marked C. The jet characteristic dimension is defined as its equivalent diameter $d_e = (4A_j/\pi)^{1/2}$, which is denoted as d for the remainder of the paper for simplicity. Also, the jet characteristic flow mass flow coefficient C_q is defined as the mass flow rate through the jet relative to the mass flow through the boundary layer across the jet's characteristic dimension (per jet), i.e., $C_q = \dot{m}_j/(\rho_0 U_0(\delta - \delta^*)d)$ where δ and δ^* are the BL thickness and displacement thickness, respectively. In the present investigation $C_q = 0.2$.

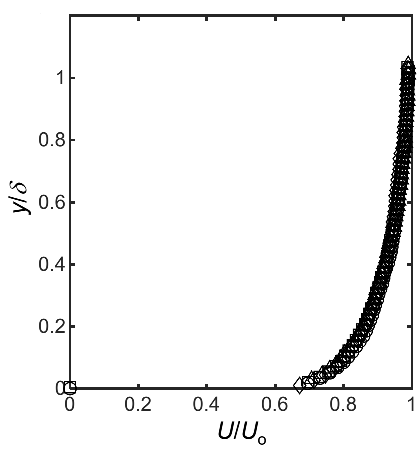

Figure 3. *Cross stream distributions of the time-averaged c streamwise velocity at x/d = 25 (Δ), 50 (□), 75 (○), and 100 (◊).*

The boundary layer of the base flow ($Re_x = 1.47\cdot10^6$ m^{-1}) was characterized at four measurement planes $x/d = 25$, 50, 75 and 100 using stereo PIV. Each vertical domain that captures the free stream at its upper edge was stitched from two partially-overlapping vertical fields. The resulting time-averaged cross stream distributions of the time-averaged streamwise velocity are shown in Figure 3. While the scaled distributions show a very close agreement, within $25 < x/d < 100$ the boundary layer's thickness δ, momentum thickness θ, and displacement thickness δ^* show small but consistent increases: $98 < \delta < 108$, $9.9 < \delta^* < 11.2$, and $7.1 < \theta < 8.1$ mm. Across the four planes, the boundary layer shape factor is invariant $h = 1.38$.

III. A Single Yawed and Non-yawed Jet

To emphasize the major differences in the interactions of a single jet with the flat-plate boundary layer, Figure 4 illustrates three characteristic flow fields in the spanwise (streamwise normal) plane $x = 50d$. In Figures 4 a and b, the circular and rectangular jets have orifices with the same d, $\alpha = 20°$ and $\beta = 60°$ with matched $C_q = 0.2$ (Toth et al., 2025a). These data show that the flow

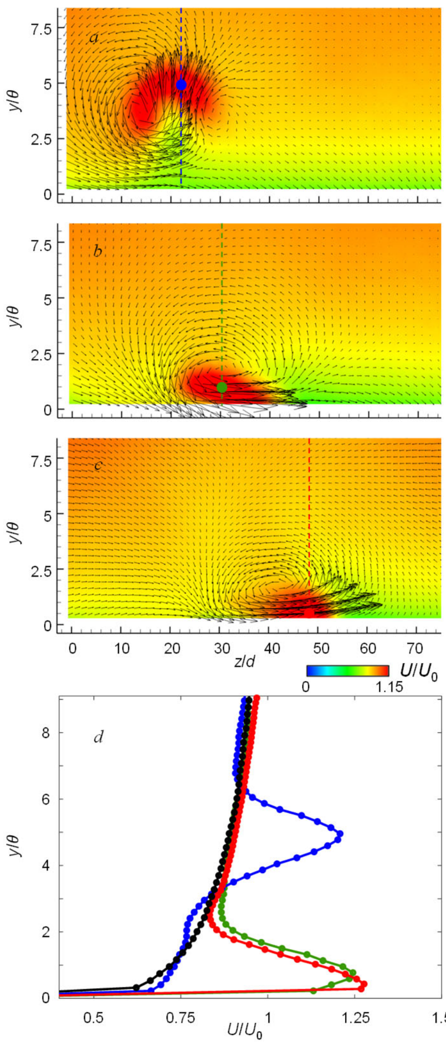

Figure 4. *Color raster plots of time-averaged streamwise velocity overlaid with in-plane velocity vectors for the circular (a), rectangular (b) and wall jet (c), and the corresponding cross stream distributions of the streamwise velocity (d): circular (●), rectangular (●), and wall jet (●) at spanwise positions of the largest velocity magnitude with jet yaw angle $\beta = 60°$, at $x/d = 50$. The base flow boundary layer (●) is shown for reference.*

fields of the jets are vastly different. The round jet forms a dominant counter-clockwise (CCW) and a weak clockwise (CW) vortex pair (Figure 4a) that is displaced above the surface and further propelled vertically by the induced joint velocity. In contrast, the corresponding rectangular jet (Figure 4b) not only results in a single CCW vortical structure, but the vortex remains close to the surface as it is advected downstream along the jet. This adherence to the surface was attributed to a Coanda effect along the long side on the downstream edge of the orifice (Toth et al., 2025a). This feature was emphasized by minimizing the jet pitch angle, rendering a wall jet whose interaction with the BL flow further promotes the adherence of the resulting vortex to the surface, as shown in Figure 4c. This CCW vortex also effects stronger lateral velocity, which is reflected in its increased spanwise displacement compared to the jet in Figure 4b. Additional illustration of the design differences between these three jet orifices is evident from distributions of the streamwise velocity in Figure 4d where each distribution is plotted at a spanwise location in Figures 4a–c that coincides with the jet core defined by the peak velocity in the flow field (marked by a dot in each of Figures 4a-c). The velocity distribution of the base flow boundary layer is included for reference. These data show that the round jet does not effect significant changes in the velocity of the base flow near the surface and its presence is centered at about $y \approx 5\theta$ with a local increase in velocity. Since the pitched rectangular jet adheres to the surface, its main contribution to the velocity is centered about $y/\theta \approx 0.7$, inducing a net velocity/momentum gain at the highest deficit of the base flow. As expected, this effect is even further augmented by the wall jet, which contributes to a peak increase in velocity/momentum peaks at $y/\theta \approx 0.4$. This design of the wall jet is used in the remainder of the current study.

Even for a rectangular wall jet, a rather dramatic difference in its evolution is seen with respect to yaw orientation, such as for the wall jets issuing streamwise ($\beta = 0$) and at yaw $\beta = 60^{\text{o}}$ that is illustrated in Figure 5 using color raster plots of the streamwise vorticity and turbulent kinetic energy (*TKE*) at $x = 75d$ from the jet orifice. At $\beta = 0$, flow around the spanwise ends of the wall jet by entrainment towards its center leads to swirling motion that gives a rise to the formation of two counter rotating streamwise edge vortices as shown in Figure 5a where the spanwise separation between the vortices indicates the spanwise extent of the jet. However, when the same jet issues at yaw $\beta = 60°$, the Coanda effect coupled with flow along the long side of the jet orifice results in the formation of a single dominant streamwise vortex with a dramatically larger characteristic scale, as shown in Figure 5b. This difference between the two vortical fields is also reflected in the distributions and magnitudes of the turbulent kinetic energy. While the TKE levels associated with vortices in either case are comparable, the peak magnitude appears to be concentrated at the joint downwash domain between the end vortices $\beta = 0$ (Figure 5c). For the single vortex at $\beta = 60°$ (Figure 5d), the elevated *TKE* is associated with the right-hand side that is characterized by intense spanwise velocity rather than on the downwash side. This brief overview clearly points to significantly different interactions of the streamwise and yawed wall jets with the surrounding boundary layer flow.

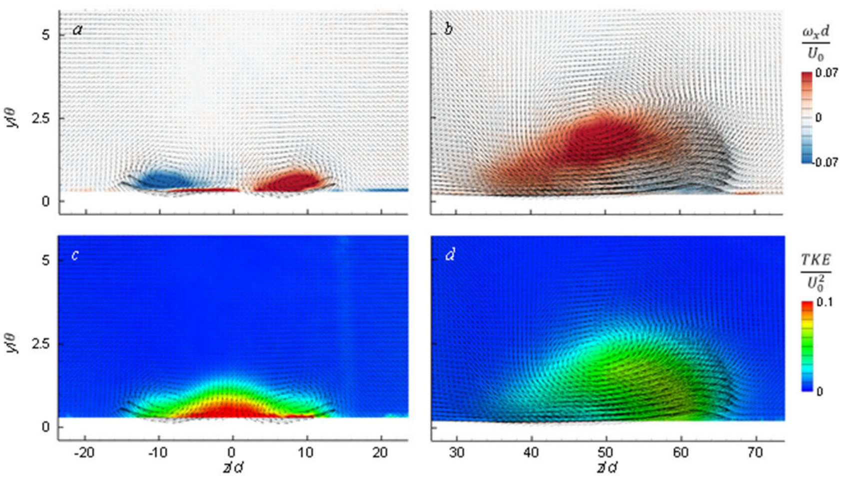

Figure 5. *Color raster plots of upstream views of time-averaged streamwise vorticity (a, b) and turbulent kinetic energy (c, d) with overlaid in-plane velocity vectors at x/d = 75: $\beta = 0°$ (a, c) and $\beta = 60°$ (b, d).*

To assess the spanwise distribution of the momentum gain due to the jet interactions with the boundary layer and its dependence on the yaw angle, it is instructive to consider the full spanwise velocity field. While the benefits of single or dual jets yawed at (or about) $\beta = 60°$ are discussed in Toth et al. (2025a, 2025b), a direct comparison of these flow fields with the non-yawed wall jet is shown in Figure 6 at $x/d = 25$, 50, 75, and 100. As expected, the wall jet issuing at zero yaw at $z/d = 0$, remains centered throughout its streamwise evolution (Figure 6i). Interestingly, its rather narrow signature at $x/d = 25$ (Figure 6i-1) continues to spread symmetrically about $z/d = 0$, while maintaining

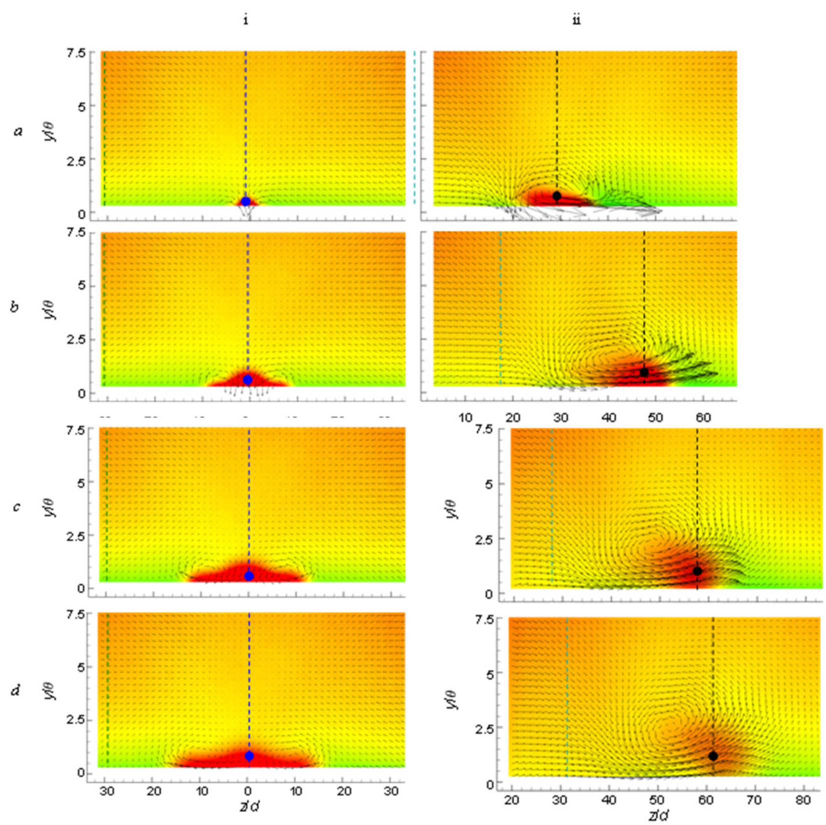

Figure 6. *Color raster plots of upstream views of time-averaged streamwise velocity overlaid with in-plane velocity vectors (as in Figure 4), at x/d = 25 (a), 50 (b), 75 (c), 100 (d), with jet yaw angles $\beta = 0°$ (Column i) and $\beta = 60°$ (Column ii). Dashed lines mark locations of the peak flow speed [marked by a dot, (—) and (—)], and in the downwash region 30d to the left (—), and (—).*

the streamwise velocity gain within a narrow region close to the surface. Thus, this gain extends over approximately a span of 30d at the farthest measured location (Figure 6i-d). However, it is also noted that past this gain, there is a rather sharp cutoff in the streamwise velocity magnitude on either side of the jet. As expected, both the signature of the streamwise velocity gain and its streamwise evolution are quite different when the same jet is yawed at $\beta = 60°$ (Figure 6ii). Although it also issues at $z/d = 0$ ($x = 0$), the yaw induces strong spanwise deflection to nearly $z/d = 30$ by the first measurement plane (Figure 6ii-a). The overall extent of the velocity gain is several times larger than for the streamwise wall jet (compared with Figure 6i-a). Another clear distinction between the downwash and upwash sides beyond the peak velocity gain is a net gain that extends past the signature of the jet on the downwash side of the embedded vortex. It is noted that the peak velocity of the jet diminishes in the streamwise direction while it continues to asymptotically deflect spanwise. The peak jet signature becomes associated with the upwash region beginning at $x/d = 50$ (Figure 6ii-c) and remains so thereafter. By $x/d = 100$, the velocity gain in the yawed jet is more diffused than in the streamwise wall jet whose contribution still remains significant and confined to the near-surface region.

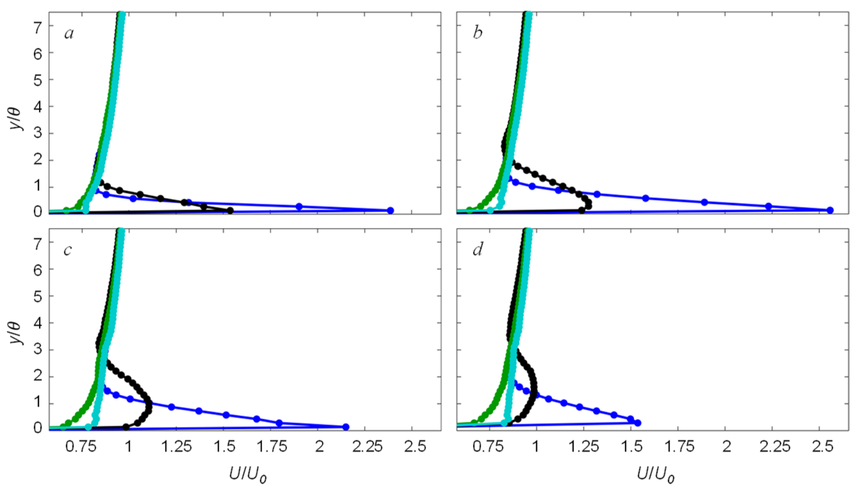

Figure 7. *Cross stream distributions of the streamwise velocity of the streamwise and yawed jets at the spanwise locations of the peak flow speed [(●), (●)] and in the downwash region 30d to the left [(●), (●)] as marked by dashed lines in Figure 6 at x/d = 25 (a), 50 (b), 75 (c), 100 (d), for β = 0°.*

To further explore the different contributions to the velocity field, a pair of streamwise velocity distributions is extracted at two spanwise positions in each of the flow fields shown in Figure 6 corresponding to the peak velocity magnitude and 30d to its left within the downwash domain of the yawed jet (both marked by dashed lines). The differences between the induced increases in streamwise velocity by the streamwise and yawed ($\beta = 60°$) wall jets are shown in Figure 7. At $x/d = 25$ (Figure 7a), the velocity distributions across the jets' peak speeds exhibit sharp peaks near the surface although the maximum velocity increase is higher in presence of the streamwise jet (2.35U_o *vs*. 1.25 U_o) but in the downwash domain 30d to the left the velocity distributions are nearly identical to the distribution of the base flow indicating nearly no effects of the jets. At $x/d = 50$ (Figure 7b), the changes induced by the yawed jet spread in the cross stream direction and its peak streamwise velocity diminishes while the peak velocity of the streamwise jet is 2.57U_o indicating that the velocity measured at $x/d = 25$ is probably not well resolved because of the proximity of the surface and its steep gradient. It is noteworthy that at this streamwise position, the effect of the yawed jet is already felt 30d on the left with an increase in the streamwise velocity near the surface but no effect of the streamwise jet. The trend of the changes induced by the yawed jet continue through $x/d = 75$ (Figure 7c), while the peak speed of the streamwise jet also diminishes. By $x/d = 100$ (Figure 7d), the velocity increase induced by the yawed jet spreads farther in the cross flow direction, extending past $y/\theta = 3$. While the velocity peak at the streamwise jet diminished to

1.5U_o, the distribution 30d to the left still shows negligible spanwise spreading indicating limited spanwise and cross stream spreading within a confined spanwise domain. In a summary, the zero-yaw jet clearly induces a strong (direct) increase in the BL velocity/momentum near the surface, but the yawed jet may be a preferable choice when uniformity of the velocity profile is of importance, in addition to greater spanwise impact and velocity/momentum gain over the baseline boundary layer.

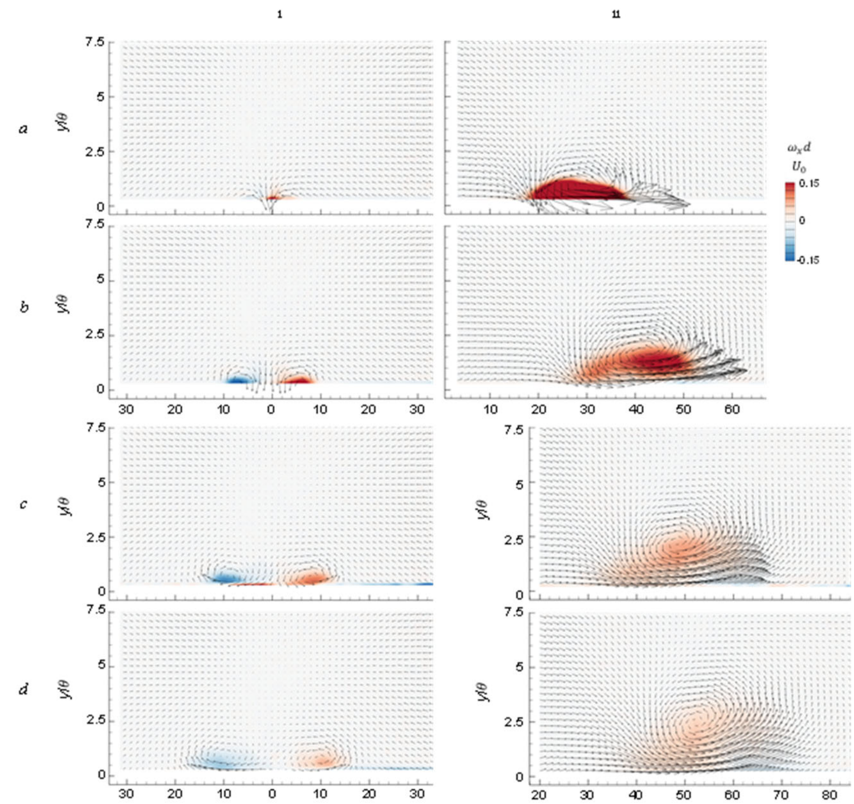

__Figure 8.__ Color raster plots of the upstream view of mean streamwise vorticity with overlaid in-pane mean velocity vectors, at x/d = 25 (a), 50 (b), 75 (c), 100 (d), with jet yaw angles yaw angles $\beta = 0°$ (i) and $\beta = 60°$ (ii).

The differences in the evolutions of the flow fields of the streamwise and yawed jets are associated with the topologies of their vorticity concentrations as already alluded to in the discussion of Figure 5. Figure 8 illustrates the fundamental differences in the vorticity fields that correspond to the jets' evolutions of Figure 6. As shown in Figure 8a, the overall scale of the streamwise vorticity concentrations of the streamwise jet at $x/d = 25$ is limited by the measurement resolution and exhibits traces of counter rotating vorticity concentrations about center span that continue to spread about the centers of their cores while they are advected spanwise along the surface in accord with their (and their image pair) induced velocity fields as shown in Figures 8i.b-d. At $x/d = 100$, the spanwise separation of the vortices is about 20d that is commensurate with the spreading of the jet. The scale of the single sense vortex formed by the yawed jet (cf. Figure 5b) at $x/d = 25$ (Figure 8ii-a) is an order of magnitude larger than the vortices induced by the streamwise jet and this CCW vortex is already displaced spanwise by nearly 30d relative to the orifice and it continues to be advected in Figures 8ii.c-d although there is clearly a streamwise diminution in the rate of spanwise advection in accord with the streamwise deflection of the yawed jet. The data in Figures 5 and 8 accentuate the changes in the flow symmetry of the streamwise jet in the presence of yaw interactions with the cross flow that are manifested by the distributions of their induced momentum fluxes as discussed in connection with Figure 9.

The interaction of the surface jets with the cross flow boundary layer can be characterized by the magnitude and spanwise distribution of the momentum flux increment $\Delta\phi = \Delta\phi(z)_x = \phi(z)_x - \phi_0(x)$ that is added to the base flow at a given spanwise position along the span by the interaction with

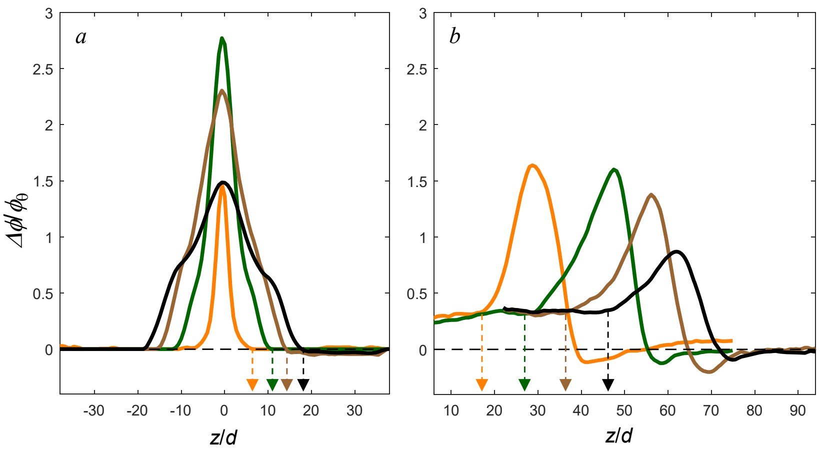

Figure 9. *Distribution of spanwise momentum flux increment* $\Delta\phi$ *relative to the momentum deficit* ϕ_θ *in the base flow boundary layer in the presence of the streamwise (a) and yawed (*$\beta = 60°$*, b) surface jets at* $x/d = 25$ *(*▬*), 50 (*▬*), 75 (*▬*), and 100 (*▬*).*

the surface jet, which is expressed relative to the momentum deficit of the baseline boundary layer flow ϕ_θ. Figure 9 shows traces of $\Delta\phi$ normalized by local momentum deficit within the baseline boundary layer $\phi_\theta(x)$ at $x/d = 25$, 50, 75, and 100 in the presence of the streamwise and yawed rectangular jets of Figure 6. As expected, the distributions of $\Delta\phi/\phi_\theta$ of the streamwise jet at $x/d = 25$ (Figure 9a) are symmetric about the jet centerline with center sharp peak and steep drop towards the spanwise edges of the jet. That the peak of $\Delta\phi/\phi_\theta$ (nearly 2.7-fold the momentum deficit of the base flow) at the centerline increases at $x/d = 50$, indicates that the trace closer to the orifice at $x/d = 25$ is probably not well-resolved due to the steep velocity gradient near surface. Farther downstream the flux peak diminishes, and the momentum increment spreads spanwise. Overall, the affected spanwise domain grows to about $\Delta z/d = 36$ at $x/d = 100$. The corresponding distributions of the yawed jet ($\beta = 60°$, Figure 9b) exhibit several distinct differences. On the downwash (left, upstream view) side of the vortex, there is a slowly varying net increase that extends outside of the measurement domain indicating an extended momentum increase to the left of the peak that further extends in z+ by about $\Delta z = 10d$ over each increment $\Delta x = 25d$ to $x/d = 100$. On the other hand, on the upwash side there is small but consistent net loss of momentum in all measurement planes ostensibly as a result of upwash of low-momentum fluid. Compared to the streamwise-oriented jet, the spanwise extent of the momentum increment effected by the yawed jet is nearly double, in concert with the differences of the induced vortical structures seen in Figure 8.

IV. Evolution of Jet Arrays

Arrays of Streamwise and Yawed Jets The interaction of spanwise arrays of the streamwise ($\beta = 0°$) and yawed ($\beta = 60°$) jets with the cross flow boundary layer was investigated using arrays of 5 jets spaced $20d$ apart and the color raster plots of the streamwise velocity at $x/d = 25$, 50, 75, and 100 are shown in Figures 10. The evolution of the array of streamwise jets is shown in Figure 10 column i. Four out of five jets in the array are captured within the field of view and the left jet at $z/d = 0$ is outside the measurement domain. These data show that jet interactions commence past $x/d = 50$ and up to this stage, each of the flow fields of the individual jets are similar to that of the single jet. The jets begin to interact along their spanwise edges where the counter-rotating edge vortices form common upwash motion while each core jet domain has a common flow down (Figures 10.i.b-d). At $x/d = 100$, the gaps of lower streamwise velocity between the jets are significantly diminished and the spanwise distribution of elevated streamwise velocity becomes more uniform. The spanwise interactions of the yawed jets commence farther upstream (Figures 10 column ii). Single jets can still be identified at $x/d = 25$ (Figure 10.ii.a), but at $x/d = 50$ (Figure

10.ii.b), the jets already interact with each other, resulting in a complete bypass of the upwash domain that is present on one side of a single jet (cf. Figure 6b-ii). Also, it is noteworthy that the end/trailing jet is directed towards its neighboring jet and begins to lose coherence. At *x*/*d* = 75 (Figure 10.ii.c), only the three left-side (upstream view) jets are visible within the field of view due to continued spanwise displacement and the trailing jet is fully drawn into its neighbor. This process clearly continues at *x*/*d* = 100 (Figure 10.ii.d), where that next induced vortex also nearly loses its coherence.

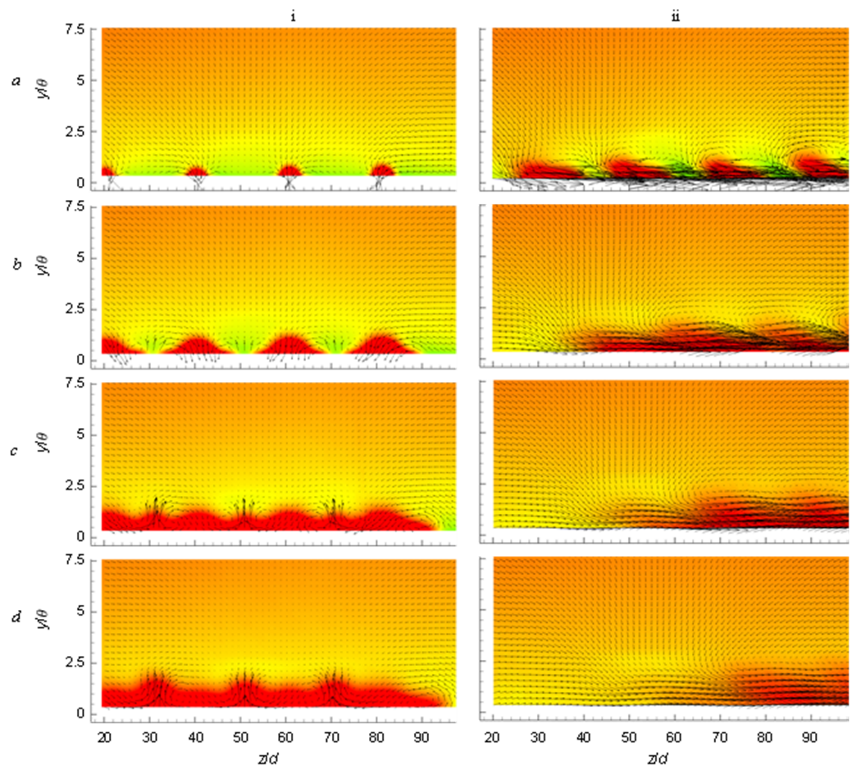

Figure 10. *Color raster plots of an upstream view of time-averaged streamwise velocity with overlaid in-plane velocity in the presence of streamwise (column i) and yawed (column ii) jets at x/d = 25 (a), 50 (b), 75 (c), and 100 (d).*

The distributions of streamwise vorticity concentrations that are associated with the flow fields in Figure 10 are shown for the streamwise and yawed jets in columns i and ii of Figure 11. As noted in connection with Figure 8.i.a, the vorticity distributions of the streamwise jet at *x*/*d* = 25 are not well resolved so Figure 11.i.a is included for reference. At *x*/*d* = 50, the end vortices between neighboring jets begin to form joint vortex pairs and induce a common upward motion in between them. This joint action intensifies by *x*/*d* = 75 (Figure 11.i.c-i), where these vortex pairs appear to intensify (ostensibly by engulfing spanwise vorticity from the boundary layer and the jet flow) and their induced upwash velocity increases. However, once these vortices are advected off the surface they become weaker, at *x*/*d* = 100. In addition to the joint vortex pairs, there is a single CCW end vortex captured within the field of view. The disparity between the vorticity distributions induced by the streamwise and yawed jets is striking as is evident in Figure 11.ii, especially at *x*/*d* = 25 (Figure 11.ii.a). Although the corresponding flow fields (Figure 10a-ii) indicate weaker interactions between the adjacent jet cores, the data in Figure 11.ii.a indicates that neighboring vortices already affect each other through interactions of their adjacent downwash and upwash domains. By *x*/*d* = 50 (Figure 11.ii.b), the vorticity concentrations are larger but more diffused and it is noted that the trailing vortex, on the left, already lost its coherence and appears to be paired with its neighbor. At *x*/*d* = 75 (Figure 11.ii.c), only three vortices remain within the field of view, where the original trailing vortex appears only as a tail of its neighbor, while the other two are visibly flattened during pairing. The pairing on the captured side of the array is mostly completed by *x*/*d* = 100 (Figure 11d-ii) and the vortices lose their coherence.

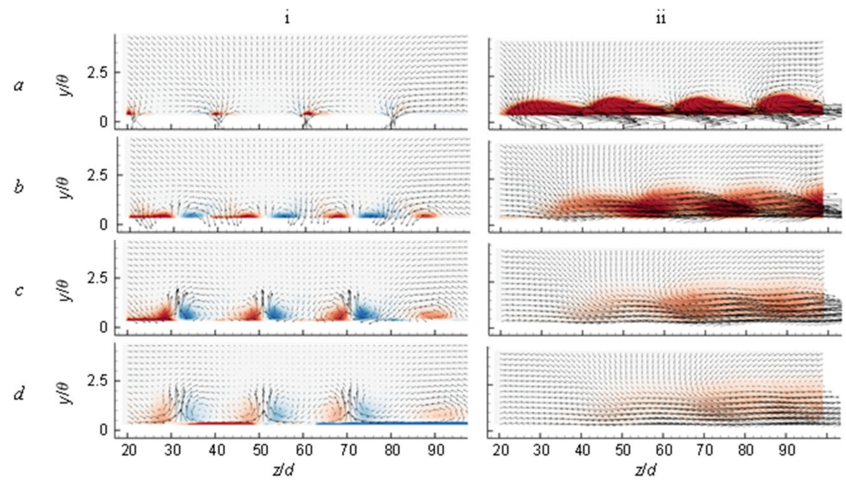

Figure 11. *Color raster plots of the upstream view of mean streamwise vorticity with overlaid in-pane mean velocity vectors at x/d = 25 (a), 50 (b), 75 (c), 100 (d), with jet yaw angles β = 0° (i) and β = 60° (ii).*

Similar to the analysis in connection with Figure 9, the ratios of the change in momentum flux across the span of the measurement domain $\Delta\phi$ to the momentum deficit of the base flow boundary layer flow ϕ_0 that is brought about by the streamwise and yawed jet arrays are shown in Figures 12a and b, respectively. The traces of $\Delta\phi/\phi_0$ for the streamwise jet at $x/d = 25$ are probably not fully-resolved, but exhibit sharp, narrow peaks that appear higher and spread somewhat by $x/d = 50$. By $x/d = 75$, spreading and interactions of adjacent jets exhibits significant overall rise in the $\Delta\phi/\phi_0$ between the jets that at $x/d = 100$ exhibit a nearly reasonably uniform level across the spanwise width of $\Delta z/d = 60$. Accounting for the trailing jet of the array that is not included in the field of view, it is estimated that the full span of $\Delta\phi/\phi_0 \approx 1.6$ is $\Delta z/d \approx 80$. The evolution of $\Delta\phi/\phi_0$ effected by the yawed jet array (Figure 12b) is clearly different. The first notable difference is visible at $x/d = 25$, where the reach of each jet is sufficiently wide to elevate the gain across the full span, including the interaction domain between the neighboring jets. The full spanwise extent of the effect cannot be captured by the present field of view since the jet array progressively shifts spanwise as the jets are advected with the flow in the streamwise direction. Nonetheless, the data show that as the jets are displaced spanwise to the left they leave a net increase across the full field of view that, at least within the field of view, asymptotes to a final gain of just below $\Delta\phi/\phi_0 \approx 0.5$ and it keeps extending in the streamwise direction with its end moving from $z/d \approx 33$ to 48, as marked by the arrows in Figure 12b. Moreover, the upper gain level rises monotonically to the right to a level of $\Delta\phi/\phi_0 \approx 1.3$.

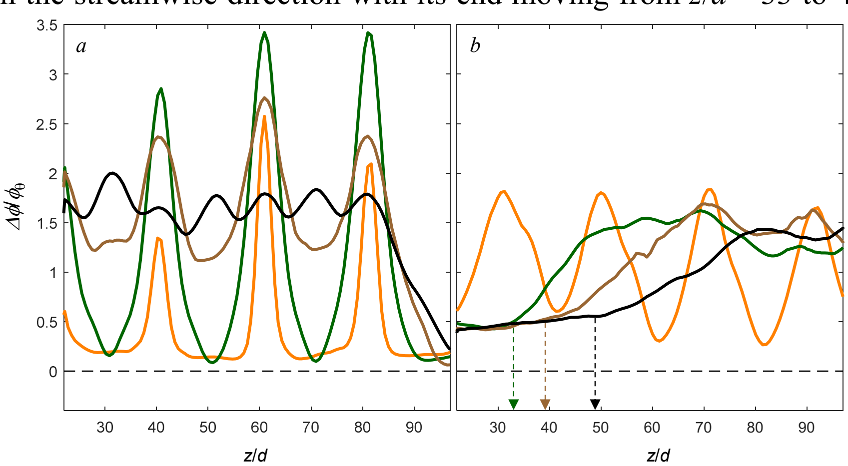

Figure 12. *Distribution of spanwise momentum flux increment Δϕ relative to the momentum deficit ϕ_θ in the base flow boundary layer in the presence of the streamwise (a) and yawed (β = 60°, b) surface jet arrays at x/d = 25 (—), 50 (—), 75 (—), and 100 (—).*

Interactions of Adjacent Yawed Jets To further assess the effects of the interactions of the yawed jets within an array, the evolution of a "minimal array" that includes three yawed jets including the leading (L) jet that issues towards the oncoming boundary layer flow, the trailing (T) jet at the opposite end and a center jet that is bound by the leading and trailing jets (C) was considered for comparison with the array of the five yawed jets ($\beta = 60°$). Figure 13 shows the evolution of a single jet (column i), for reference, 3-jet array (column ii), and 5-jet array (column iii). The evolution of the single jet was discussed in connection with Figure 6 with emphasis on its surface adherence and the upwash and downwash flows of its vortex. When considering evolution of an array of three jets (Figures 13.ii), some subtle differences, depending on the jet position in the array are noted at $x/d = 25$ (Figure 13a-ii). The upwash domains of both the trailing (T) and central (C) vortices are suppressed due to the interactions with neighboring vortices, while only the leading vortex (L) still induces a notable upwash motion in addition to the strong spanwise component. Furthermore, interactions between the downwash and upwash domains of the T-C and C-L jets leaves only the downwash domain of the trailing vortex. While the leading vortex of the five-jet array is outside of the field of view (Figures 13.iii), the same T-C jet interaction is visible and is further evident in the central C-C jet interactions. By $x/d = 50$ (Figures 13b-ii and 13b-iii), the trailing-jet vortex already lost its coherence, while the joint structure of T-C and C-C jet vortices indicate a complete bypass of flow upwash while retaining a strong spanwise velocity component. The only exception is the leading vortex that, due to presence of upwash on its outer side grows somewhat larger than the other remaining vortices. At $x/d = 75$ (Figures 13.ii.c and 13.iii.c), the remnant of the trailing vortex appears only as a trail of velocity increase, while the other vortices, except the leading vortex (Figure 13.ii.c), almost lost their coherence and have an elongated core. To emphasize uniqueness of the leading vortex, a dashed line connects it to the single vortex in Figure 13.i.c, as the evolution of the leading vortex resembles that of the single vortex. Even when all the other vortices lose their coherence at $x/d = 100$, a partial capture of the leading vortex in Figure 13d-ii still suggests its resilience, in spite of interactions with the merged remnants of the other vortices on its downwash side.

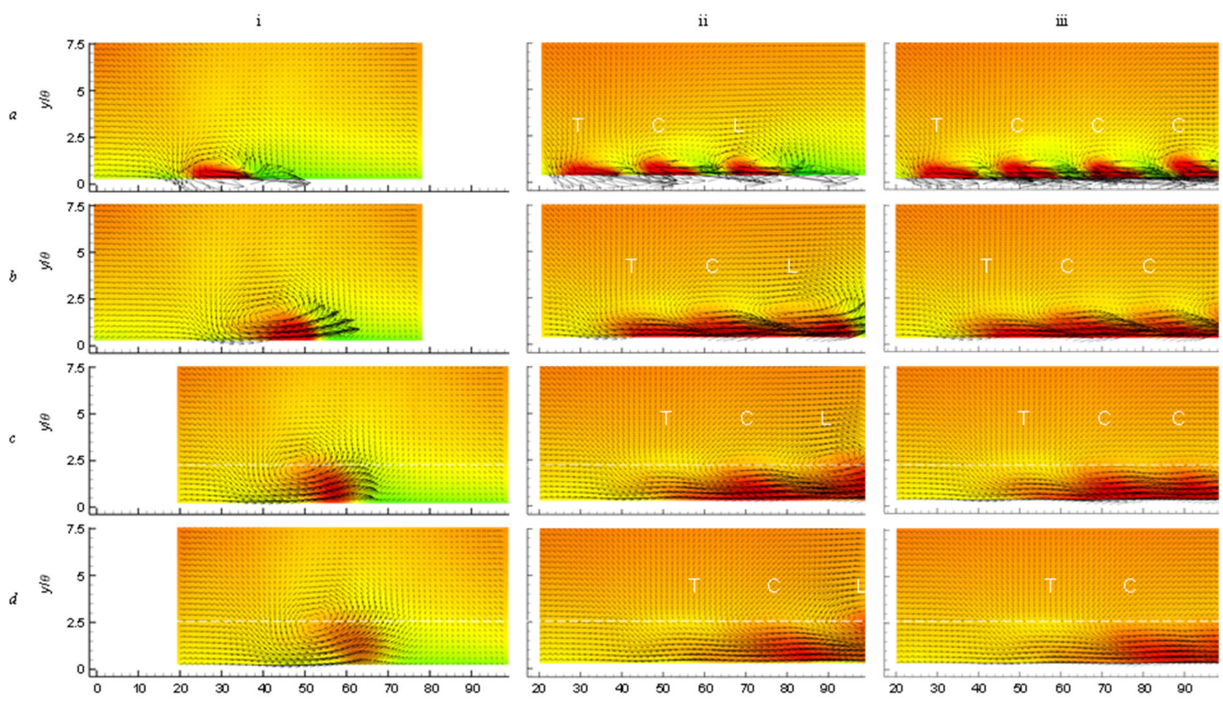

__Figure 13.__ Color raster plots of the upstream view of mean streamwise velocity with overlaid in-pane mean velocity vectors for n = 1 (i), 3 (ii), and 5 (iii) wall jets ($\beta = 60°$) at x/d = 25 (a), 50 (b), 75 (c), 100 (d).

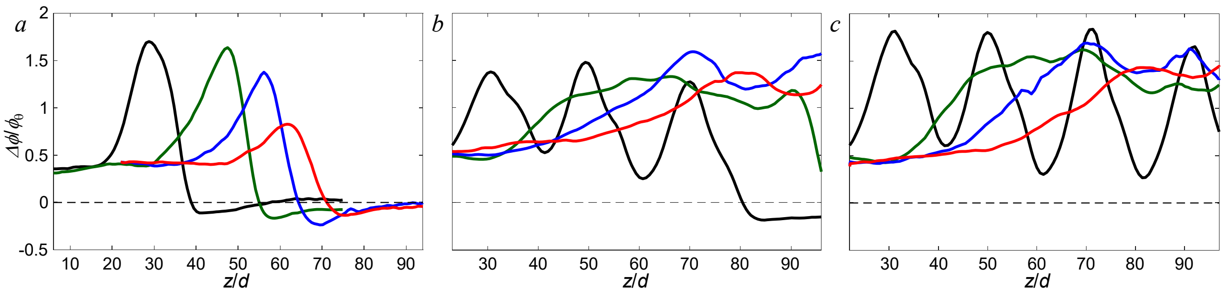

Figure 14. *Distribution of spanwise momentum flux increment Δφ relative to the momentum deficit ϕ_θ in the base flow boundary layer of the in the presence of yawed (β = 60°) single jet (a), 3-jet array (b), and 5-jet (c) array at x/d = 25 (—) 50 (—) 75 (—) and 100 (—).*

The contributions of jet-array interactions shown in Figure 13 to the net gain in momentum flux are quantified in Figure 14. The distributions of the single yawed jet that were discussed in connection with Figure 9b are shown in Figure 14a for reference. Different effects on the downwash and upwash side of the vortex are quantified in the asymptotic net gain on the downwash side that extends in the spanwise direction with streamwise advection, and a small net deficit on the upwash side that propagates with the vortex displacement. Analysis of the corresponding evolutions for the three- and five-jet arrays in Figures 14b and c, respectively, point to similar developments on the trailing-jet side of the array, especially at the two streamwise planes where the leading jet of the three-jet array is partially or completely outside of the field of view. Clearly, the three-jet array displays all the specific features of the evolutions of a T-C-L jet combination that is particularly visible at $x/d = 50$ in Figure 14b, where the tail-end asymptotic leveling is visible in association with the folding of the trailing vortex, to the drop off at the opposite end due to flow upwash of the leading vortex. It is worth noting that the asymptotic leveling at higher magnitude than for a single vortex (Figure 14a), as it is assisted by the interaction with the neighboring vortices, while addition of central vortices as in the five-jet array (Figure 14c) does not seem to affect this plateau reached by the three-jet array.

V. Conclusions

The interactions of spanwise arrays of 3-D surface wall jets with a cross flow of a flat plate turbulent boundary layer ($Re_x = O[10^6]$) were investigated in wind tunnel experiments. Each wall jets issues out of rectangular orifice in the surface of the plate that can be yawed relative to the free stream. The orifice characteristic scale, measured by its equivalent diameter d (d_e) was an order of magnitude smaller than boundary layer thickness and the jets adhere to the surface by a Coanda effect along the downstream edge of the orifice and remain in close proximity to the surface within the wall layer over 100 equivalent orifice diameters. When the jet is yawed, it forms a single-sense, surface-bound vortex that remains close to the surface as it is advected downstream along with the jet. The present investigations focused primarily on comparison between arrays of streamwise ($\beta = 0°$) and yawed ($\beta = 60°$) jets that led to markedly different flow topologies with significant ramifications to spanwise distributions of their induced increments of momentum flux within the boundary layer. The evolution of the near-surface flow field in the absence and presence of the jets was measured using stereo PIV in four streamwise-normal planes $x/d = 25$, 50, 75, and 100 downstream from the jet orifices.

The present investigations showed that the evolutions and structure of isolated streamwise and yawed ($\beta = 60°$) jets within the boundary layer are strikingly different. While the streamwise rectangular jet remains confined to the surface and forms relatively weak counter rotating edge vortices, the yawed jet forms a strong single-sense streamwise vortex with significant induced upwash and downwash flows. Furthermore, the streamwise jet induces strong, but spanwise limited, momentum increments within the wall region, and the yawed jet leads to momentum distribution that is far reaching across the span, particularly on the downwash side of its single-sense vortex.

The evolution of adjacent streamwise jets is driven by their spanwise proximity. Once their spanwise spreading results in interactions of the counter rotating edge vortices from neighboring jets, they couple into vortex pairs having common induced upwash that promotes a transfer of the elevated near-wall momentum from each jet into the gap between them leading to increased streamwise momentum flux while flattening the jet cores, coupled with some growth and advection of the edge vortices. Interactions between yawed jets in the array commence significantly closer to their orifices, where single-sense vortices in close proximity override the upwash action of their neighbors yielding a common momentum flux enhancement across the affected boundary layer span. Consequently, although attaining that through different mechanisms, both the yawed and streamwise jet arrays can effect nearly uniform net spanwise gain of streamwise momentum flux that occurs closer to the array's orifices for the yawed jets that reach an asymptotic net gain of close to 50% of the boundary layer's momentum deficit. The increase in momentum flux by distributed streamwise jets occurs farther downstream although the velocity within the inner layer remain significantly overshooting the free stream speed. This overshoot may relax farther downstream and result in a more balanced TBL velocity profiles.

Finally, analysis of the streamwise evolutions of single, three, and five yawed jets, shows differences in interactions of the jets bound by neighboring jets. It is shown that when the jets are yawed, the evolution of the jets in an array depends on whether the jet is bound by the neighboring jets, or whether it points into the oncoming boundary layer (referred to as 'leading') or towards a neighboring jet (referred to as 'trailing'). The trailing jet leads the interactions with its neighboring central jet, followed by interactions among the central jets, while the leading jet retains the most streamwise coherence, being similar in its evolution to an isolated jet.

Acknowledgment/Disclaimer

This work was sponsored by the Office of Naval Research (ONR), under grant number N000142312500. The views and conclusions contained herein are those of the authors only and should not be interpreted as representing those of ONR, the U.S. Navy, or the U.S. Government.

References

Berger, P. A. and Liburdy, J. A., "A Near-Field Investigation into the Effects of Geometry and Compound Angle on the Flowfield of a Row of Film Cooling Holes," ASME Paper 98-GT-279, 1998.

Cerretelli, C., and Williamson, C. H. K., "The Physical Mechanism for Vortex Merging," *Journal of Fluid Mechanics*, Vol. 475, 2003, pp. 41–77.

Compton, D.A. and Johnston, J.P., "Streamwise Vortex Production by Pitched and Skewed Jets in a Turbulent Boundary Layer," *AIAA Journal*, Vol. 30, 1992, pp.640-647.

Findlay, M. J., Salcudean, M., and Gartshore, I. S., "Jets in a Crossflow: Effects of Geometry and Blowing Ratio," *Journal of Fluids Engineering*, Vol. 121, No. 2, 1999, pp. 373–378.

Gutmark, E. J., and Grinstein, F. F., "Flow Control with Noncircular Jets," *Annual Review of Fluid*

Mechanics, Vol. 31, 1999, pp. 239–272.

Johnston, J. P., and Nishi, M., Vortex Generator Jets – Means for Flow Separation Control, *AIAA Journal,* Vol. 28, 1990, pp. 989–994.

Johnston, J.P. "Pitched and Skewed Vortex Generator Jets for Control of Turbulent Boundary Layer Separation: A Review," Proceedings of the 3rd ASME/JSME Joint Fluids Engineering Conference, FEDSM99-6917, 1999.

Karagozian, A.R., "The Jet in Crossflow," *Physics of Fluids*, Vol. 26, No. 10, 2014, pp.1-47.

Mahesh, K., "The Interaction of Jets with Crossflow," *Annual Review of Fluid Mechanics*, Vol. 45, 2013, pp. 379-407.

Margason, R. J., "Fifty Years of Jet in Crossflow Research," In Computational and Experimental Assessment of Jets in Cross Flow, *AGARD-CP-534*, 1993.

Milanovic, I.M. and Zaman, K. B. M. Q., "Fluid Dynamics of Highly Pitched and Yawed Jets in Crossflow," *AIAA Journal*, Vol. 42, No. 5, 2004, pp. 874 - 882.

Pauley, W. R. and Eaton, J. K., "Experimental Study of the Development of Longitudinal Vortex Pairs Embedded in a Turbulent Boundary Layer," *AIAA Journal*, Vol. 26, 1988, pp. 816-823.

Ramaswamy, D.P. and Schreyer, A.M., "Control of Shock-induced Separation of a Turbulent Boundary Layer using Air-jet Vortex Generators. *AIAA Journal*, Vol. 59, 2021, pp.927-939.

Sharmishtha, C. and Utpal, B., "Review of Jets in a Cross Flow-Experimental and Numerical Approach," *International Journal of Engineering and Advanced Technology*, Vol. 7, No. 2, 2017, pp. 114-128.

Sterland, P. R. and Hollingsworth, M. A., "An Experimental Study of Multiple Jets Directed Normally to a Cross-Flow," *Journal of Mechanical Engineering Science*, Vol. 17, No. 3, 1975, pp. 117-124.

Toth, B., Vukasinovic, B., Glezer, A., DeFore, M.C., and Harris, C., "Interactions of Controlled Streamwise Vortices with a Turbulent Boundary Layer," AIAA Paper 2025-1489, 2025a.

Toth, B., Vukasinovic, B., Glezer, A., DeFore, M.C., and Harris, C., "Wall-Bound Streamwise Vortices formed by Embedded Jets in a Turbulent Boundary Layer," AIAA Paper 2025-3394, 2025b.

Verma, S.B. and Manisankar, C., "Control of Compression-ramp-induced Interaction with Steady Microjets, *AIAA Journal*, Vol. 57, 2019, pp. 2892-2904.

Zhang, X. "An Inclined Rectangular Jet in a Turbulent Boundary Layer—Vortex Flow," *Experiments in Fluids*, Vol. 28, 2000, pp. 344–354.